IEEE Access
Multidisciplinary ⋮ Rapid Review ⋮ Open Access Journal

Received 2 June 2022, accepted 17 June 2022, date of publication 27 June 2022, date of current version 1 July 2022.

Digital Object Identifier 10.1109/ACCESS.2022.3186363

Efficient 3D Image Reconstruction for Near-Field Microwave Imaging Using Dynamic Metasurface Antenna

AMIR MASOUD MOLAEI, VASILIKI SKOUROLIAKOU, VINCENT FUSCO, (Fellow, IEEE), AND OKAN YURDUSEVEN, (Senior Member, IEEE)

Institute of Electronics, Communications and Information Technology (ECIT), Queen's University Belfast, Belfast BT3 9DT, U.K.

Corresponding author: Amir Masoud Molaei (a.molaei@qub.ac.uk)

This work was supported by the Leverhulme Trust under Research Leadership under Award RL-2019-019.

ABSTRACT In this paper, rapid reconstruction of a three-dimensional (3D) image of a scene for near-field microwave imaging using a dynamic metasurface antenna (DMA) is addressed. The imaging system consists of a fixed transmitting DMA and a single moving antenna as the receiver. In the proposed approach, after pre-processing the raw data and converting it into an applicable form for Fourier computations, the converted data are processed by the presented algorithm (all with fast Fourier computations, without the need for the heavy Stolt interpolation step). Furthermore, after extracting a closed-form expression for image reconstruction, a minimization problem is defined using the compressive-sensing (CS) theory, which allows a sparse pattern to be sampled instead of collecting full data, thereby significantly improving the data acquisition rate (according to the CS rate). The performance of the proposed approach is examined by computer simulations and analytical discussions.

INDEX TERMS 3D microwave imaging, compressive-sensing, dynamic metasurface antenna, fast Fourier computations.

I. INTRODUCTION

In recent decades, the widespread applications of microwave imaging in areas such as security screening, medical imaging, nondestructive testing and evaluation, structural health monitoring, and through-wall imaging have led to significant advances in various layers of imaging radars, from the physical layer to the system and signal processing layers [1], [2]. In imaging systems, gathering the scene data is usually done either by mechanical scanning or by electronic scanning (large phased arrays with independent antennas) [3], [4]. Although the electronic scanning mechanism may be a suitable solution to improve the data acquisition rate, phased array antennas may be expensive and bulky. In addition, due to the need for complex control circuitry and a large number of radio frequency discrete components (such as amplifiers, attenuators, filters, phase shifters, etc.), they usually suffer from high power consumption.

The associate editor coordinating the review of this manuscript and approving it for publication was Qingchun Chen.

As an alternative to conventional imaging techniques, some modern computational imaging schemes [5] such as coded aperture [6] and single-pixel [7] modalities with relaxed hardware constraints have been used. Recently, dynamic metasurface antenna (DMA) has been proposed as an effective platform for computational microwave imaging [8], [9]. DMA contains a waveguide with subwavelength metamaterial elements called unit-cells [10]. The DMA can produce different radiation patterns even at a single frequency [9]. This is because unit-cells can be actively modulated throughout the metasurface [11].

Although employing DMAs simplifies the hardware part, they do not produce uniform radiation patterns due to physical layer compression. As a result, the raw information provided by them cannot be directly processed by efficient computational Fourier transform (FT)-based scene reconstruction techniques. This can limit the advantage of fast Fourier calculations for an imaging system with a DMA transmitter (Tx) or receiver (Rx). To address this issue, in [12]–[14], an effective solution compatible with the range migration algorithm

(RMA) [15] is presented that allows the expression of DMA-derived measurements in the spatial-frequency domain and the transformation of raw data on Fourier bases. The system layouts studied in [12]–[14] involve using a DMA panel aperture as Tx and a probe antenna as Rx, which essentially represents a panel-to-probe architecture. Therefore, to reconstruct a three-dimensional (3D) scene, the transceiver system needs to perform a full mechanical scanning in numerous uniform spatial-frequency steps. This is a major challenge for real-time applications in terms of the data acquisition rate as well as for implementation. Also, the image reconstruction process requires a Stolt interpolation step [16], which is the most complex computational part of RMA-based techniques.

To address the above two issues, in this paper, we propose an approach based on fast Fourier and sparse sampling without Stolt interpolation (which we call FFSSWSI). In the proposed approach, by defining a minimization problem based on compressive-sensing (CS), only a limited share of total spatial-frequency data will be required. This allows us to skip the full scanning without having to worry about violating the Nyquist criterion (either in the spatial or frequency domain), and thus significantly increase the data acquisition rate. Also, in the image reconstruction section for computational efficiency, we define a nonuniform inverse fast Fourier transform (NUIFFT)-based process that replaces the heavy Stolt interpolation step. The performance of the FFSSWSI approach will be analyzed by computer simulations.

The rest of this paper is organized as follows: Section II details the proposed approach, including the system and data model, and image reconstruction algorithm; Section III is devoted to presenting the results and discussion; finally, Section IV provides the concluding remarks.

Notation: Throughout the paper, symbols $(\cdot)^{\dagger}$, $\|\cdot\|_p$ and j stand for the pseudoinverse, ℓ_p-norm and the imaginary unit, respectively.

II. PROPOSED APPROACH

A. SYSTEM AND DATA MODEL

Fig. 1 shows an overview of the imaging system studied in this paper. This system uses a fixed DMA along the x-axis (horizontal) as the Tx. This DMA consists of a 1D microstrip waveguide with N_T complimentary electric-LC resonators placed at a subwavelength spacing from each other [17]. Each element can be randomly turned on/off by an external stimulus. This can lead to the production of a set of masks (corresponding to diverse and distinct spatial radiation patterns). Leveraging this concept, at a given frequency f, multiple measurements can be provided by cycling through M masks (tuning states). As a Rx, a single antenna moves along the y-axis (vertical) to receive the backscattered signal. As a rule, to observe the Nyquist rate and also to benefit from fast Fourier calculations, it is necessary to perform this vertical scanning evenly and with limited intervals. However, this can greatly increase the data acquisition time. We assume here that both spatial and frequency sampling are performed

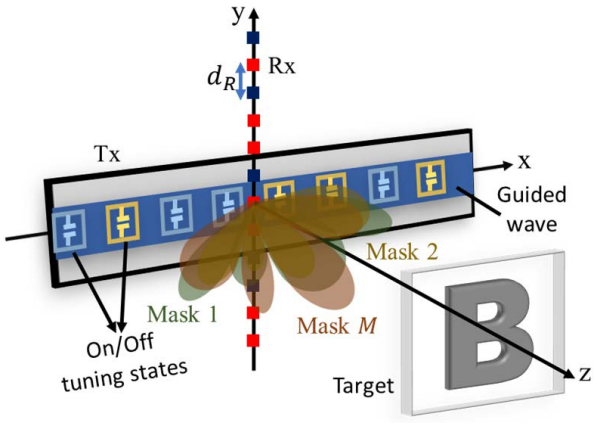

FIGURE 1. Overview of the imaging system.

non-uniformly (randomly) with a much smaller number of samples (with a specified CS rate) compared to full sampling. As an example depiction of the sparse sampling process, Fig. 1 shows the mechanical scanning points in blue and the omitted points in red.

Since the DMA cannot be modeled as a single dipole, the measurement signal g (given below) has a more complex form than the total field that is conventionally calculated only by the Green's function G [12], [13]

$$g(f) = \int_V U_T(\vec{r}; f)\, \rho(\vec{r})\, G(y_R, \vec{r}; f)\, dV, \tag{1}$$

where $dV = dxdydz$, y_R corresponds to the position of Rx, ρ represents the reflectivity of the target, and $\vec{r}$ is the position vector to a point in the scene. In the above equation, U_T is the radiated field from the aperture, which can be expressed as the superposition of all metamaterial elements (see [12], [13] for more details).

B. IMAGE RECONSTRUCTION

Assuming that the signal measured in the aperture plane can be expanded in terms of the fields corresponding to all the masks, we can write [12], [13]

$$g_{m,i'}(f) = \sum_{i=1}^{N_T} \Phi_m(x_i; f)\, s(x_i, y_{i'}; f),$$
$$m = 1, \ldots, M,\ i' = 1, \ldots, N_R, \tag{2}$$

where Φ_m and s represents the field over the aperture for the m-th mask and total field (incident field), respectively. N_R denotes the number of vertical scanning points. By creating a set of aperture modes with some degrees of orthogonality, using the delta function screening property and applying some mathematical simplifications, (2) can be written in matrix form as follows:

$$\mathbf{s}(f) = \mathbf{\Phi}^{\dagger}(f)\, \mathbf{g}(f), \tag{3}$$

where $\mathbf{g}(f) \in C^{M \times N_R}$, $\mathbf{\Phi}(f) \in C^{M \times N_T}$ and $\mathbf{s}(f) \in C^{N_T \times N_R}$. The data is now in the form needed to introduce and apply a fast Fourier-based technique. Therefore, according to the

above and the geometry of the system, the received signal can be considered as

$$s\left(x_T,\, y_R;\, f\right) = \int_V \frac{\rho\left(x,\, y,\, z\right)}{16\pi^2 R_T R_R} e^{-jkR_T} e^{-jkR_R} \delta\left(y_T,\, z_T\right) \delta\left(x_R,\, z_R\right) dV, \tag{4}$$

where $(x_T,\, y_T,\, z_T)$ and $(x_R,\, y_R,\, z_R)$ correspond to the positions of Tx and Rx. Also, R_T and R_R represent the distances between the positions of Tx and Rx to the target points, respectively. By taking the 2D FT from both sides of (4) on the aperture coordinates, employing the convolution theorem and method of stationary phase [18] and applying some mathematical approximations and simplifications, the signal representation in the wavenumber domain can be written as follows (see [12], [19] for details):

$$S\left(k_x,\, k_y,\, k\right) = \frac{-j}{32\pi k \left(k^2 - k_x^2\right)^{\frac{1}{4}} \left(k^2 - k_y^2\right)^{\frac{1}{4}}} \times \int_x \int_y \int_z \rho\left(x,\, y,\, z\right) e^{-jk_x x} e^{-jk_y y} e^{-j\left(\sqrt{k^2-k_x^2}+\sqrt{k^2-k_y^2}\right)z} \times dz dy dx,\, k^2 \geq k_x^2,\, k^2 \geq k_y^2. \tag{5}$$

In the above equation, the term $-j\pi / \left(2k \left(k^2 - k_x^2\right)^{1/4} \left(k^2 - k_y^2\right)^{1/4}\right)$ acts as a filter in the Fourier domain. Also, from the above equation, it can be concluded that to retrieve the target reflectivity, a 3D inverse Fourier transform must be applied to the signal $\bar{S}\left(k_x,\, k_y,\, k_z\right)$, where $\bar{S}\left(k_x,\, k_y,\, k_z\right)$ is the signal mapped from $S\left(k_x,\, k_y,\, k\right)$ upon defining $k_z \sqrt{k^2 - k_x^2} + \sqrt{k^2 - k_y^2}$ with an equispaced distribution. Such mapping is known in the literature as Stolt interpolation [16]. Stolt interpolation is computationally the most expensive step of image reconstruction in RMA-based techniques. In the following, we intend to solve this problem by replacing the interpolation step with a less computationally expensive mechanism while improving the data acquisition rate according to the structure introduced in Section II-A.

Suppose we denote the output signal obtained by applying filtering to $S\left(k_x,\, k_y,\, k\right)$ with $\tilde{S}\left(k_x,\, k_y,\, k\right)$. This filtering is performed by using the appropriate amplitude term mentioned above as well as backpropagating the signal to the center of the scene in the range z_0 (also called motion compensation). Motion compensation corrects the wavefront curvature of all scatterers at the same range as the scene center [20]. In this way, we can rewrite (5) as follows:

$$\rho\left(x,\, y,\, z\right) = \int_{dk_x} \int_{dk_y} \int_{dk} \tilde{S}\left(k_x,\, k_y,\, k\right) e^{jk_x x} e^{jk_y y} e^{j\left(\sqrt{k^2-k_x^2}+\sqrt{k^2-k_y^2}\right)z} \times dk dk_y dk_x, \tag{6}$$

and by discretizing it in spatial and spectral domains, we have

$$\rho\left(x_p,\, y_{p'},\, z_{p''}\right) = \sum_{q=1}^{N_{kx}} \sum_{q'=1}^{N_{ky}} \sum_{q''=1}^{N_{kz}} \tilde{S}\left(k_{x,\,q},\, k_{y,\,q'},\, k_{q''}\right) e^{jk_{x,\,q} x_p} e^{jk_{y,\,q'} y_{p'}} e^{jk_{z,\,q''} z_{p''}},$$
$$p = 1,\, \ldots,\, N_x,\, p' = 1,\, \ldots,\, N_y,\, p'' = 1,\, \ldots,\, N_z, \tag{7}$$

where $k_{z,\,q'} \triangleq \sqrt{k_{q''}^2 - k_{x,\,q}^2} + \sqrt{k_{q''}^2 - k_{y,\,q'}^2}$, and N_{kx}, N_{ky} and N_{kz} are the number of samples corresponding to the wavenumbers. Also, $N_x \times N_y \times N_z$ indicates the number of voxels in the imaging scene. To benefit from the computational advantage of IFFT, the samples of $\left\{k_{x,\,1},\, \ldots,\, k_{x,\,N_{kx}}\right\}$ and $\left\{k_{y,\,1},\, \ldots,\, k_{y,\,N_{ky}}\right\}$ must be considered with uniform spacing. This, assuming that the distribution of k is uniform, leads to non-equispaced samples of $\left\{k_{z,\,1},\, \ldots,\, k_{z,\,N_{kz}}\right\}$ and prevents direct use of the IFFT operator. Therefore, we adapt the NUIFFT operator to our problem to take advantage of fast calculations in the Fourier domain for inner summation in (7) without the need for a heavy Stolt interpolation step

$$\rho\left(x,\, y,\, z\right) = \mathrm{IFFT}_{k_x,\,k_y} \left\{\widehat{s}\left(k_x,\, k_y,\, z\right)\right\}, \tag{8}$$

where

$$\widehat{s}\left(k_{x,\,q},\, k_{y,\,q'},\, z\right) \triangleq \mathrm{NUIFFT}_{k_z} \left\{\tilde{S}\left(k_{x,\,q},\, k_{y,\,q'},\, k\right)\right\}, \quad q = 1,\, \ldots,\, N_x,\, q' = 1,\, \ldots,\, N_y. \tag{9}$$

Details of implementing a 1D NUIFFT operator can be found in detail in [21], [22]. Therefore, according to the above, the relationship between the measurement data and the reconstructed image in the introduced system can be written in the following closed-form expression:

$$\rho\left(x_p,\, y_{p'},\, z_{p''}\right) = \mathrm{IFFT}_{k_x,\,k_y} \times \left\{\mathrm{NUIFFT}_{k_z} \left\{\mathrm{Filter} \left\{\mathrm{FFT}_{x,\,y} \times \left\{\boldsymbol{\Phi}^{\dagger}\left(f_l\right) \mathbf{g}\left(y_{i'};\, f_l\right)\right\}\right\}\right\}\right\}, \quad l = 1,\, \ldots,\, N_f, \tag{10}$$

where N_f denotes the total number of frequency samples. As mentioned in the previous sections, the introduced system does not provide the desired data acquisition rate due to numerous scanning points in the vertical direction and the need for many frequency samples. We address this issue by defining a minimization problem using CS theory and based on the relation extracted in (10) so that there is no need to collect numerous data at the Nyquist rate. Assume that $\mathbf{s}$ exhibits sparsity on a certain orthonormal basis $\boldsymbol{\Psi}$. By arranging $\mathbf{s}$ as a columnar vector (i.e. $\check{\mathbf{s}} \in C^{N_T N_R N_f \times 1}$), it can be represented by using its sparse transform domain vector $\boldsymbol{\theta}$ as a compressible signal [23], [24]

$$\check{\mathbf{s}} = \boldsymbol{\Psi}_{N_T N_R N_f \times N_T N_R N_f} \boldsymbol{\theta}_{N_T N_R N_f \times 1}. \tag{11}$$

Let us denote the set of randomly selected reduced measurements by

$$\mathbf{s}'\left(f\right) \triangleq \boldsymbol{\Phi}'^{\dagger}\left(f\right) \mathbf{g}'\left(f\right), \tag{12}$$

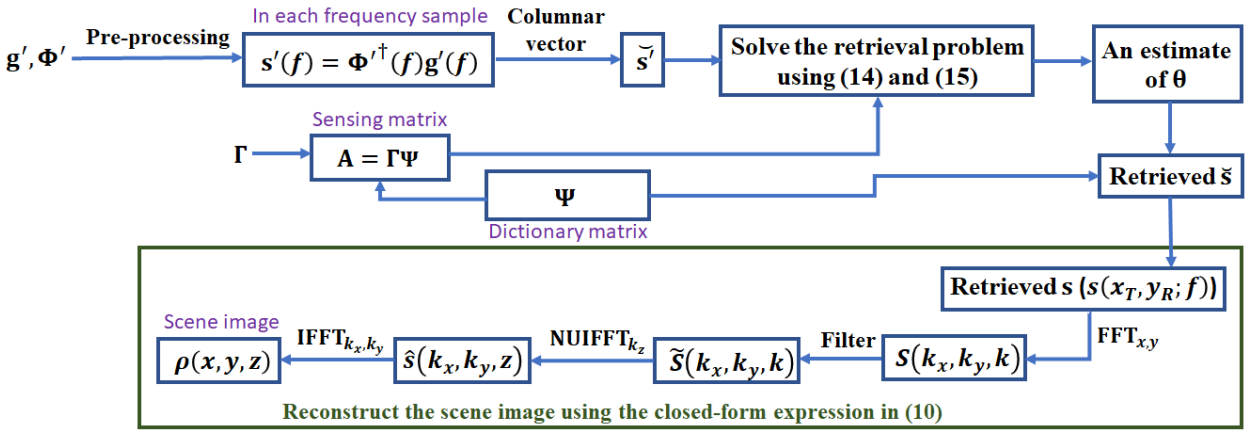

FIGURE 2. Flow diagram of the main steps of implementing the proposed approach.

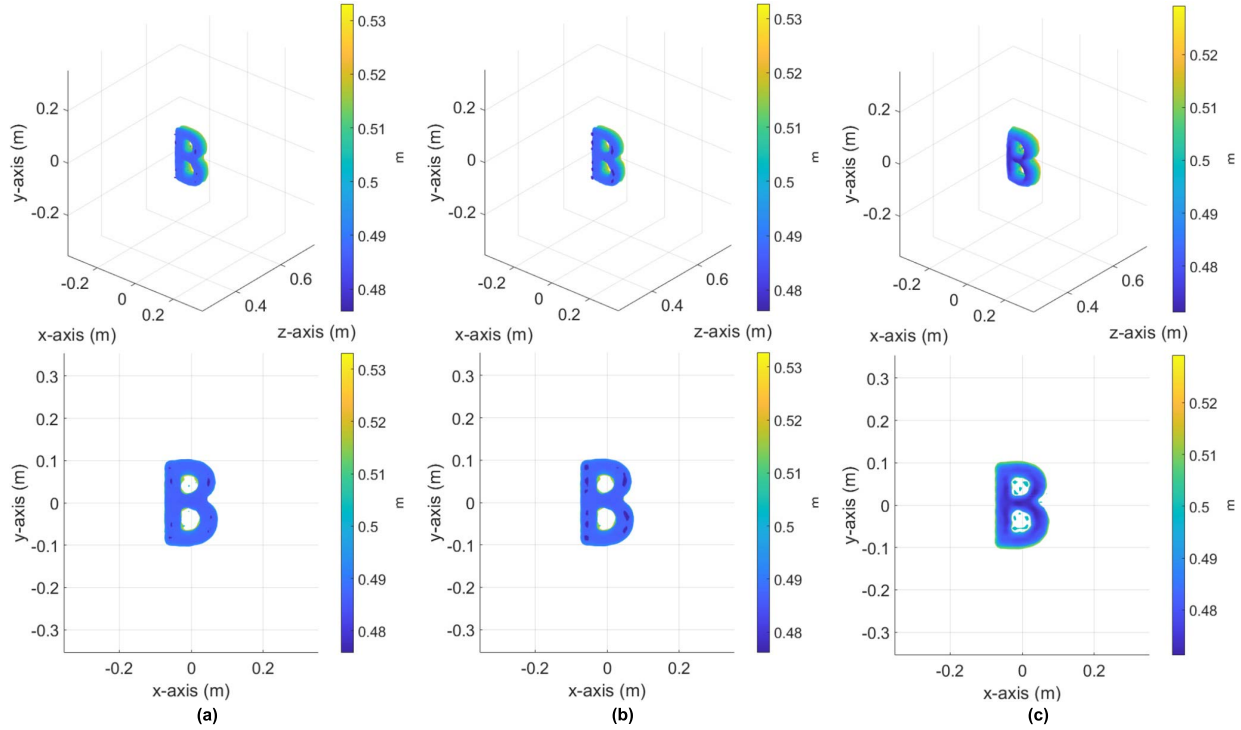

FIGURE 3. Reconstructed images in 3D and 2D views; (a) by algorithm [12], [13] using the spline interpolation method, (b) by algorithm [12], [13] using the interpolation method in (16), (c) by the proposed approach. Isovalue: −10 dB. Colorbar denotes the range distance.

where $\mathbf{g}' \in \mathbb{C}^{M\times M_R\times M_f}$, $\mathbf{\Phi}' \in \mathbb{C}^{M\times N_T\times M_f}$, $\mathbf{s}' \in \mathbb{C}^{N_T\times M_R\times M_f}$, $M_R < N_R$ and $M_f < N_f$. Note that $\mathbf{g}'(f) \in \mathbb{C}^{M\times M_R}$, $\mathbf{\Phi}'(f) \in \mathbb{C}^{M\times N_T}$ and $\mathbf{s}'(f) \in \mathbb{C}^{N_T\times M_R}$ represent the values of $\mathbf{g}'$, $\mathbf{\Phi}'$, $\mathbf{s}'$ in each frequency sample, respectively. According to (11), columnar vector of $\mathbf{s}'$ (i.e. $\breve{\mathbf{s}}' \in \mathbb{C}^{N_T M_R M_f\times 1}$) can be modeled by projections of $\check{\mathbf{s}}$ onto vectors $\{\gamma_1, \ldots, \gamma_{N_T M_R M_f}\}$ constituting the measurement matrix $\mathbf{\Gamma}$ as

$$\breve{\mathbf{s}}' = \mathbf{\Gamma}_{N_T M_R M_f\times N_T N_R N_f}\check{\mathbf{s}} = \mathbf{A}_{N_T M_R M_f\times N_T N_R N_f}\boldsymbol{\theta}, \quad (13)$$

where $\mathbf{A} = \mathbf{\Gamma}\mathbf{\Psi}$ is the sensing matrix. The recovery problem can be described as the following convex ℓ_1-minimization [25]:

$$\min \|\boldsymbol{\theta}\|_1 \quad \text{s.t. } \breve{\mathbf{s}}' = \boldsymbol{\theta}. \quad (14)$$

To solve (14), we define a cost function as follows [26]:

$$E(\boldsymbol{\theta}) = \frac{1}{2}\left\|\breve{\mathbf{s}}' - \mathbf{A}\boldsymbol{\theta}\right\|_2^2 + \alpha\|\boldsymbol{\theta}\|_1, \quad (15)$$

where α is the regularization parameter that controls the relative weight of the two terms. Details of implementation are provided in Section III.

By solving the above problem, $\mathbf{s}$ can be retrieved with much less data (according to CS theory), and then the scene

TABLE 1. Simulation parameters.

Parameter	f	N_f	$N_T = N_R$	$d_T = d_R$	Q	M	z_0	α
Value	17.5-22 GHz	51	105	6.81 mm ($\lambda/2$)	50	105	0.5 m	0.001

image can be reconstructed by using (10). A summary of the main steps of implementing the proposed approach with the variables introduced above is given in the form of a block diagram in Fig. 2.

III. SIMULATION RESULTS AND DISCUSSION

All computations are performed on a MATLAB R2020b platform running on a 64-bit Windows 10 operating system with 12GB of random-access memory and a Core-i7 central processing unit at 2.7GHz. To implement NUIFFT, a fast Gaussian gridding-based method is used, which includes the main steps of initialization, convolution, IFFT and deconvolution [27]. Γ is designed so that only one 1 is randomly (with a uniform distribution) placed in each row, and the rest of the entries are 0. For the dictionary matrix, we considered the discrete Fourier transform domain, which provided the best performance compared to the discrete cosine transform and wavelet domains in our experiments. To minimize the cost function in (15), we used the two-step iterative shrinkage/thresholding (TwIST) algorithm [28], which converges much faster than similar algorithms such as IST [29].

The simulation parameters are given in Table 1, where Q is the quality factor of the metamaterial elements [30] and λ is the wavelength corresponding to the highest frequency in free space. In each mask, half of the elements are randomly turned on. In all experiments, a 3D B-shaped distributed target (see Fig. 1) is considered. Due to the size of the aperture (0.71×0.71 m^2) and the operating frequency, targets with a range of less than approximately 66m are located in the near-field (NF) region [31].

First, we compare the performance of the image reconstruction algorithm presented in this paper with the adapted RMA in [12], [13] without sparse data (with full data). Note that since the geometry of the imaging system in this work is somewhat different from the work [12], [13], we adapted the algorithm [12], [13] based on the geometry of Fig. 1 to make a fair comparison. Figs. 3(a) and 3(b) show the outputs of the algorithm [12], [13] as isosurfaces of the normalized image when using the spline interpolation [32] and an interpolation method with a simpler implementation based on the minimum distance criterion (given below), respectively:

$$\begin{aligned}\hat{S}\left(k_{x,q},\, k_{y,q'},\, k_{z,q''}\right) &= \hat{S}\left(k_{x,q},\, k_{y,q'},\, k_{z,q''}\right) + \tilde{S}\left(k_{x,q},\, k_{y,q'},\, k_l\right), \\ &\arg\min_{q''}\left|k_{z,q''} - \sqrt{k_l^2 - k_{x,q}^2} - \sqrt{k_l^2 - k_{y,q'}^2}\right|, \quad (16)\end{aligned}$$

where $q'' = 1, \ldots, N_z$ and $\hat{S}$ is initialized to zero. The reconstructed images are displayed in 3D and 2D (xy-plane) views. Note that the images are distance color-coded and the colorbar represents the range in meters.

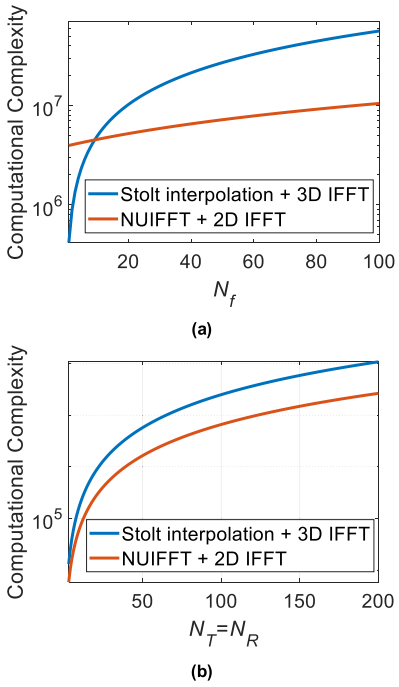

FIGURE 4. Comparison of the computational complexity of two different schemes; (a) versus N_f, (b) versus $N_T = N_R$.

It can be seen that Fig. 3(b) has fewer sidelobes than Fig. 3(a), however, it requires more computational time. The average computational times for the interpolation and 3D IFFT steps for Figs. 3(a) and 3(b) are calculated as 1.03 and 0.86 seconds, respectively. Fig. 3(c) shows the corresponding outputs obtained by the FFSSWSI approach. The target image is well reconstructed and completely recognizable. Although the reconstructed image is less focused along the z-axis than in Figs. 3(a) and 3(b), the average computational time of alternative operations (1D NUIFFT + 2D IFFT instead of Stolt interpolation + 3D IFFT) is 0.63 seconds, which shows the computational superiority of the proposed approach.

To validate this observation analytically, we extracted the major computational complexity of the above operations. Stolt interpolation + 3D IFFT requires $\mathcal{O}\big(N_T N_R \left(n^2 N_f + N_I \log\left(N_I N_T N_R\right)\right)\big)$ arithmetic operations, where N_I and n represent the number of sampling points in interpolation and spline function order, respectively; while 1D NUIFFT + 2D IFFT employed in the proposed approach requires $\mathcal{O}\big(N_T N_R \big(M_{sp} N_f + 0.5 M_r log M_r + \log\left(N_T N_R\right)\big)\big)$ operations, where M_{sp} and M_r represent spreading parameter and oversampling number, respectively. Fig. 4 shows a comparison of the computational complexity between the two schemes versus different numbers of frequency and spatial samples. As can be seen, the scheme employed in the proposed approach shows much better computational performance than the conventional interpolation-based scheme, especially when the number of samples increases. In addition,

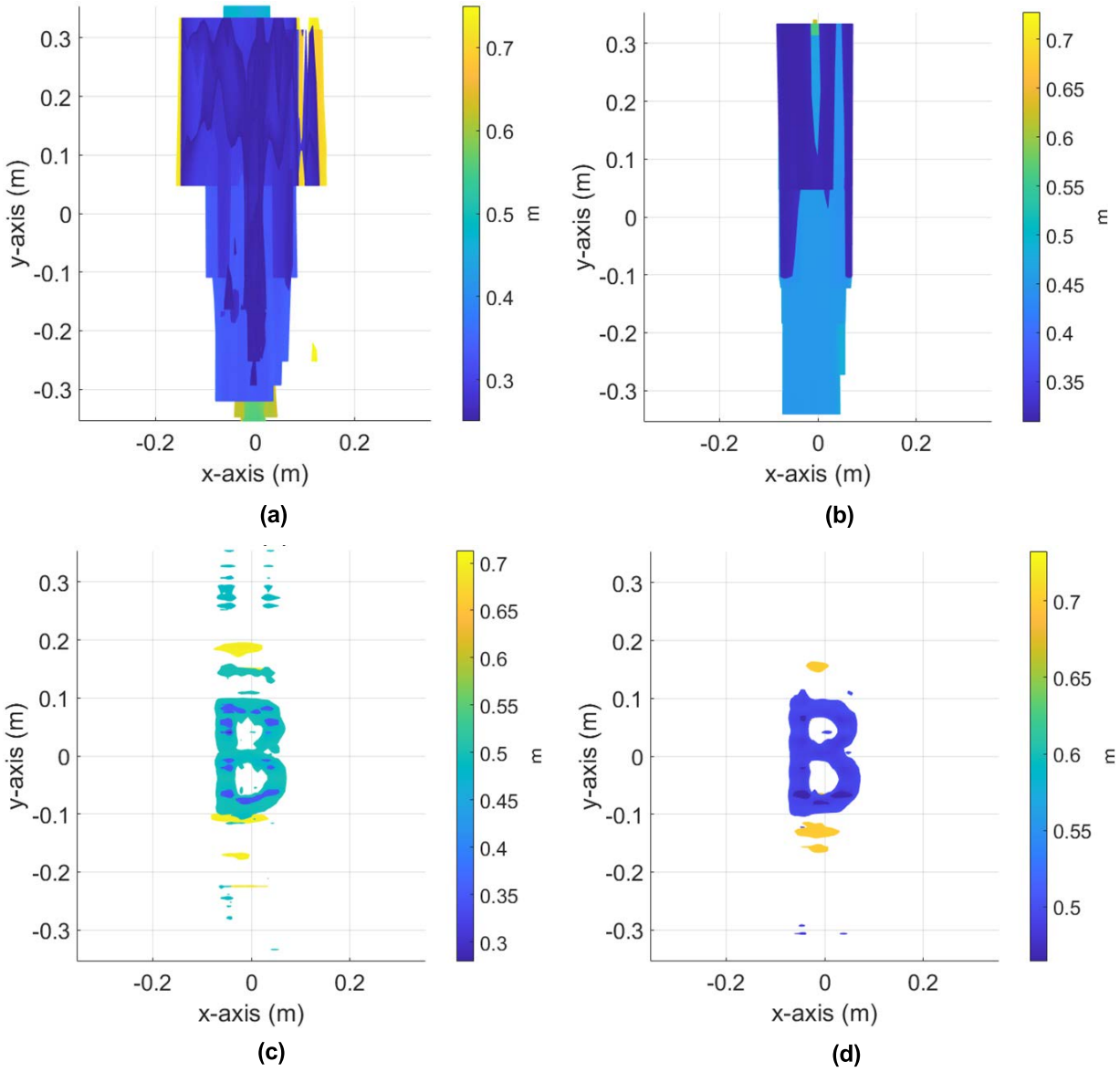

FIGURE 5. Reconstructed images using sparse data; (a) by adapted RMA, CS rate: 25%, (b) by adapted RMA, CS rate: 42.25%, (c) by the proposed approach, CS rate: 25%, (d) by the proposed approach, CS rate: 42.25%. Isovalue: −9 dB. Colorbar denotes the range distance.

TABLE 2. Comparison of computational time, NMSE, contrast and entropy values corresponding to Fig. 3.

	Fig. 3(a)	Fig. 3(b)	Fig. 3(c)
Involved Steps	Spline interpolation and 3D IFFT	Interpolation method in (16) and 3D IFFT	1D NUIFFT and 2D IFFT
Computation Time	1.03 Sec	0.86 Sec	0.63 Sec
NMSE	Reference image	0.041	0.045
Contrast	110.27	108.95	104.89
Entropy	5.14	5.22	5.24

in Table 2, we calculated the normalized mean squared error (NMSE) values [4], [24] and summarized them with the computational times mentioned above. To calculate the NMSE, Fig. 3(a) is taken as the reference image. The NMSE value calculated for Fig. 3(c) is very close to that for Fig. 3(b), which can be verified by visual inspection of the figures. Furthermore, Table 2 provides the image contrast and entropy values [33]–[35] averaged from 2D reconstructed images (on the xy-plane) focused in different ranges. These results agree with the above findings in terms of the performance of various techniques.

In addition to the experiments performed on the full data, we also examined the performance of the FFSSWSI approach on the spatial-spectral sparse data and compared the results with the adapted RMA method. Figs. 5(a) and 5(b) show the reconstructed images by the adapted RMA method, when $M_R = 0.5N_R$, $M_f = 0.5N_f$, and $M_R = 0.65N_R$, $M_f = 0.65N_f$, respectively. These values are equivalent to CS rates of 25% and 42.25%, respectively. As expected, due to

TABLE 3. The values of computational time, NMSE, contrast and entropy corresponding to Fig. 5 (Fig. 3(a) is used as the reference image for the NMSE calculation).

Figure	5(a)	5(b)	5(c)	5(d)
NMSE	0.311	0.163	0.111	0.075
Contrast	59.43	66.45	79.88	91.86
Entropy	6.27	6.02	5.62	5.47

non-compliance with the Nyquist criterion in both spatial and frequency sampling, the resulting images are aliased and the target is not recognizable. Also, as can be seen, the deviation from the target position is much more severe in the y- and z-axes, because the sparse data are related to mechanical scanning samples in the y-direction and frequency samples (which contain the range information), but in the horizontal direction, the full data (DMA related data) are used. The corresponding images, when the proposed approach is used, are shown in Figs. 5(c) and 5(d). Although these images contain some undesirable sidelobes, unlike Figs. 5(a) and 5(b), the target image is well recognizable. Also, by comparing Figs. 5(a) and 5(b), it is clear that increasing the CS rate can be effective in improving the quality of the reconstructed image; however, this comes at the cost of increasing the number of measurements (reducing the data acquisition rate). Table 3 lists the NMSE, contrast and entropy values, which are consistent with the findings in Fig. 5 and the description above. As the CS rate increases, the error value decreases, the contrast improves, and the entropy value, which is interpreted here as the degree of irregularity (heterogeneity), decreases [33]–[35].

IV. CONCLUSION

An effective approach to 3D image reconstruction in a NF microwave imaging system including a DMA was addressed. The most important achievement of this work is to formulate a solution to match the sparse data (instead of the full measurements) and to eliminate the Stolt interpolation step by replacing it with a more efficient computational process (fast Fourier type). The results of simulations and computational analyses showed that using the proposed approach, a 3D image of the scene can be reconstructed faster than conventional RMA-based methods. Adapting the solution with sparse data can lead to an improved data acquisition rate (proportional to CS rate) in the introduced system.

REFERENCES

[1] W. Shao and T. McCollough, "Advances in microwave near-field imaging: Prototypes, systems, and applications," *IEEE Microw. Mag.*, vol. 21, no. 5, pp. 94–119, May 2020.

[2] P. Kiran, "Microwave imaging," *Int. Res. J. Eng. Technol.*, vol. 7, no. 5, pp. 251–256, 2020.

[3] A. M. Molaei, O. Yurduseven, and V. Fusco, "An efficient waveform diversity based on variational mode decomposition of coded beat-frequency shifted signals algorithm for multiple-input multiple-output millimetre-wave imaging," *IET Radar, Sonar Navigat.*, vol. 15, no. 10, pp. 1266–1280, Oct. 2021.

[4] A. M. Molaei, S. Hu, V. Skouroliakou, V. Fusco, X. Chen, and O. Yurduseven, "Fast processing approach for near-field terahertz imaging with linear sparse periodic array," *IEEE Sensors J.*, vol. 22, no. 5, pp. 4410–4424, Mar. 2022.

[5] N. Sarhangnejad, N. Katic, Z. Xia, M. Wei, N. Gusev, G. Dutta, R. Gulve, H. Haim, M. M. Garcia, D. Stoppa, K. N. Kutulakos, and R. Genov, "5.5 dual-tap pipelined-code-memory coded-exposure-pixel CMOS image sensor for multi-exposure single-frame computational imaging," in *IEEE Int. Solid-State Circuits Conf. (ISSCC) Dig. Tech. Papers*, Feb. 2019, pp. 102–104.

[6] X. Liu, H. Wang, C. Luo, and L. Peng, "Terahertz coded-aperture imaging for moving targets based on an incoherent detection array," *Appl. Opt.*, vol. 60, no. 23, pp. 6809–6817, 2021.

[7] O. Yurduseven, M. A. B. Abbasi, T. Fromenteze, and V. Fusco, "Lens-loaded coded aperture with increased information capacity for computational microwave imaging," *Remote Sens.*, vol. 12, no. 9, p. 1531, May 2020.

[8] T. A. Sleasman, M. F. Imani, A. V. Diebold, M. Boyarsky, K. P. Trofatter, and D. R. Smith, "Implementation and characterization of a two-dimensional printed circuit dynamic metasurface aperture for computational microwave imaging," *IEEE Trans. Antennas Propag.*, vol. 69, no. 4, pp. 2151–2164, Apr. 2021.

[9] M. F. Imani, J. N. Gollub, O. Yurduseven, A. V. Diebold, M. Boyarsky, T. Fromenteze, L. Pulido-Mancera, T. Sleasman, and D. R. Smith, "Review of metasurface antennas for computational microwave imaging," *IEEE Trans. Antennas Propag.*, vol. 68, no. 3, pp. 1860–1875, Mar. 2020.

[10] M. Jian, G. C. Alexandropoulos, E. Basar, C. Huang, R. Liu, Y. Liu, and C. Yuen, "Reconfigurable intelligent surfaces for wireless communications: Overview of hardware designs, channel models, and estimation techniques," 2022, *arXiv:2203.03176*.

[11] T. Sleasman, *Dynamic Metasurface Apertures for Computational Imaging*. Durham, NC, USA: Duke Univ., 2018.

[12] L. Pulido-Mancera, T. Fromenteze, T. Sleasman, M. Boyarsky, M. F. Imani, M. Reynolds, and D. Smith, "Application of range migration algorithms to imaging with a dynamic metasurface antenna," *J. Opt. Soc. Amer. B, Opt. Phys.*, vol. 33, no. 10, pp. 2082–2092, Oct. 2016.

[13] L. M. P. Mancera, *Analytical Modeling of Waveguide-fed Metasurfaces for Microwave Imaging and Beamforming*. Durham, NC, USA: Duke Univ., 2018.

[14] A. V. Diebold, L. Pulido-Mancera, T. Sleasman, M. Boyarsky, M. F. Imani, and D. R. Smith, "Generalized range migration algorithm for synthetic aperture radar image reconstruction of metasurface antenna measurements," *J. Opt. Soc. Amer. B, Opt. Phys.*, vol. 34, no. 12, pp. 2610–2623, Dec. 2017.

[15] Z. Manzoor, M. T. A. Qaseer, and K. M. Donnell, "A comprehensive bi-static amplitude compensated range migration algorithm (AC-RMA)," *IEEE Trans. Image Process.*, vol. 30, pp. 7038–7049, 2021.

[16] S. Jiacheng and M. Chen, "Research on imaging algorithm of millimeter wave radar based on stolt interpolation," in *IEEE MTT-S Int. Microw. Symp. Dig.*, May 2019, pp. 1–4.

[17] I. Yoo, *Analytic Model, Design of Waveguide-Fed Metasurface Antennas and Applications to MIMO Communication Systems*. Durham, NC, USA: Duke Univ., 2020.

[18] X. Nie, C. Lin, and A. Qing, "FFT-SAR algorithm for MIMO system based on stationary phase method," in *Proc. IEEE Asia–Pacific Microw. Conf. (APMC)*, Dec. 2020, pp. 863–865.

[19] X. Chen, Q. Yang, B. Deng, Y. Zeng, and H. Wang, "A FFT-based millimeter-wave imaging algorithm with range compensation for near-field MIMO-SAR," *J. Infr., Millim., THz Waves*, vol. 42, no. 4, pp. 391–408, Apr. 2021.

[20] J. M. Lopez-Sanchez and J. Fortuny-Guasch, "3-D radar imaging using range migration techniques," *IEEE Trans. Antennas Propag.*, vol. 48, no. 5, pp. 728–737, May 2000.

[21] S. Wang, Y. Fang, J. Zhang, M. Luo, and Q. Li, "Near-field 3D imaging approach combining MJSR and FGG-NUFFT," *J. Syst. Eng. Electron.*, vol. 30, no. 6, pp. 1096–1109, 2019.

[22] Y. Jiang, H. Fan, H. Wang, and B. Deng, "Experimental study of azimuth-elevation three-dimensional imaging at terahertz frequencies," in *Proc. IET Int. Radar Conf. (IET IRC)*, Nov. 2021, pp. 1037–1039.

[23] S. Bennett, Y. Noblet, P. F. Griffin, P. Murray, S. Marshall, J. Jeffers, and D. Oi, "Compressive sampling using a pushframe camera," *IEEE Trans. Comput. Imag.*, vol. 7, pp. 1069–1079, 2021.

[24] A. M. Molaei, S. Hu, V. Skouroliakou, V. Fusco, X. Chen, and O. Yurduseven, "Fourier compatible near-field multiple-input multiple-output terahertz imaging with sparse non-uniform apertures," *IEEE Access*, vol. 9, pp. 157278–157294, 2021.

[25] S. Mousavi and J. Shen, "Solution uniqueness of convex piecewise affine functions based optimization with applications to constrained ℓ_1 minimization," *ESAIM, Control, Optim. Calculus Variat.*, vol. 25, p. 56, Jan. 2019.
[26] C. Huang, H. Ji, J. Qiu, L. Wang, and X. Wang, "TwIST sparse regularization method using cubic B-spline dual scaling functions for impact force identification," *Mech. Syst. Signal Process.*, vol. 167, Mar. 2022, Art. no. 108451.
[27] C. Eleftheriadis and G. Karakonstantis, "Fast and accurate power spectral analysis of heart rate variability using fast Gaussian gridding," in *Proc. Comput. Cardiology (CinC)*, Sep. 2021, pp. 1–4.
[28] S. Li, J. N. Chen, H. Wang, and Z. Cui, "An image reconstruction algorithm based on two-step iterative shrinkage/thresholding for electrical resistance tomography," in *Proc. IEEE Int. Instrum. Meas. Technol. Conf. (I2MTC)*, May 2021, pp. 1–5.
[29] D. Kim and D. Park, "Element-wise adaptive thresholds for learned iterative shrinkage thresholding algorithms," *IEEE Access*, vol. 8, pp. 45874–45886, 2020.
[30] M. Askari, H. Pakarzadeh, and F. Shokrgozar, "High Q-factor terahertz metamaterial for superior refractive index sensing," *J. Opt. Soc. Amer. B, Opt. Phys.*, vol. 38, no. 12, pp. 3929–3936, 2021.
[31] A. M. Molaei, P. del Hougne, V. Fusco, and O. Yurduseven, "Efficient joint estimation of DOA, range and reflectivity in near-field by using mixed-order statistics and a symmetric MIMO array," *IEEE Trans. Veh. Technol.*, vol. 71, no. 3, pp. 2824–2842, Mar. 2022.
[32] F. Krieg, J. Kirchhof, F. Romer, A. Ihlow, G. Del Galdo, and A. Osman, "Implementation issues of 3D SAFT in time and frequency domain for the fast inspection of heavy plates," in *Proc. IEEE Int. Ultrason. Symp. (IUS)*, Sep. 2017, pp. 1–4.
[33] X. Mao, X. He, and D. Li, "Knowledge-aided 2-D autofocus for spotlight SAR range migration algorithm imagery," *IEEE Trans. Geosci. Remote Sens.*, vol. 56, no. 9, pp. 5458–5470, Sep. 2018.
[34] M. K. Newey, J. M. Kantor, and G. R. Benitz, "Autofocus methods for moving target imaging in synthetic aperture radar," *IEEE Trans. Geosci. Remote Sens.*, vol. 60, pp. 1–11, 2022.
[35] J. M. Kantor, "Differentiable synthetic aperture radar image formation and generalized minimum entropy autofocus," in *Proc. IEEE Radar Conf. (RadarConf)*, May 2021, pp. 1–6.

AMIR MASOUD MOLAEI was born in Tehran, Iran, in 1987. He received the B.Sc. degree in communications engineering and the M.Sc. degree in telecommunication systems engineering from the Sahand University of Technology, Tabriz, Iran, in 2010 and 2013, respectively, and the Ph.D. degree in telecommunication systems engineering from the Babol Noshirvani University of Technology (BNUT), Babol, Iran, in 2019.

From 2015 to 2019, he was a Lecturer with the Faculty of Electrical Engineering, BNUT; the Mazandaran Institute of Technology; and Islamic Azad University. During the period 2019–2020, he has joined Future Wave Ultratech Company as a Mobile Networks (GSM/UMTS/LTE) Analyzer and Planner. He is currently with the Centre for Wireless Innovation, School of Electronics, Electrical Engineering and Computer Science, Queen's University Belfast, as a Postdoctoral Research Fellow. He was ranked first in the Ph.D. entrance exam in telecommunication systems at BNUT and ranked first among the Ph.D. graduates from the Telecommunication Engineering Department. He has published over 35 refereed papers and has filed two patents. His current research interests include signal processing, radar imaging algorithms, and sensor arrays.

Dr. Molaei is the General Chair of the 2022 International Conference on Manufacturing, Industrial Automation and Electronics (ICMIAE 2022). He has served as a Senior Editor for the *Cloud Computing and Data Science* (CCDS). He has also served as a Technical Reviewer for numerous prestigious leading journals, including IEEE Wireless Communications, IEEE Transactions on Vehicular Technology, and IEEE Transactions on Automation Science and Engineering.

VASILIKI SKOUROLIAKOU received the integrated M.Sc. degree in electrical and computer engineering from the University of Thessaly, Volos, Greece, in 2019. She is currently pursuing the Ph.D. degree with the Institute of Electronics, Communication and Information Technology, Queen's University Belfast, U.K.

Her current research interests include signal processing algorithms for millimeter-wave radars, image reconstruction techniques, real-time algorithm implementation-code acceleration techniques, and development of EM numerical models.

VINCENT FUSCO (Fellow, IEEE) received the bachelor's degree (Hons.) in electrical and electronic engineering, the Ph.D. degree in microwave electronics, and the D.Sc. degree from Queen's University Belfast (QUB), Belfast, U.K., in 1979, 1982, and 2000, respectively. He is currently the Director of research with the ECIT Research Institute, QUB. He specializes in microwave through millimeter front-end circuit architectures. He has made numerous contributions to this field and holds several fundamental patents on self-tracking antennas and high-performance micromachined frequency selective surfaces. He has published over 650 peer-reviewed research papers, two books, and holds 12 patents. He is a member of the Royal Irish Academy and a fellow of the Royal Society, U.K. Royal Academy of Engineering, the Irish Academy of Engineering, and the Institution of Engineering and Technology (IET). He is also a Chartered Engineer. In 2012, he was awarded the IET Senior Achievement Award, the Mountbatten Medal, and the Royal Irish Academy Gold Medal for Engineering Sciences, in 2019.

OKAN YURDUSEVEN (Senior Member, IEEE) received the B.Sc. and M.Sc. degrees in electrical engineering from Yildiz Technical University, Istanbul, Turkey, in 2009 and 2011, respectively, and the Ph.D. degree in electrical engineering from Northumbria University, Newcastle upon Tyne, U.K., in 2014.

From 2014 to 2018, he was a Postdoctoral Research Associate at Duke University. From 2018 to 2019, he was a NASA Research Fellow at the Jet Propulsion Laboratory, California Institute of Technology, USA. He is currently a Reader (an Associate Professor) at the School of Electronics, Electrical Engineering and Computer Science, Queen's University Belfast, U.K. He is also an Adjunct Professor at Duke University, USA. He has authored more than 150 peer-reviewed technical journals and conference papers. He has been the principal investigator on research grants totaling in excess of two million GBP in these fields. His research interests include microwave and millimeter-wave imaging, multiple-input-multiple-output (MIMO) radars, wireless power transfer, antennas and propagation, and metamaterials.

Dr. Yurduseven is a member of the European Association on Antennas and Propagation (EurAAP). He has been serving as a Technical Program Committee Member for the SPIE Defense and Commercial Sensing Conference, since 2020. He was a recipient of several awards, including an Outstanding Postdoctoral Researcher Award at Duke University, in 2017; the Duke University Professional Development Award, in 2017; the NASA Postdoctoral Program Award, in 2018; the British Council—Alliance Hubert Curien Award, in 2019; the Leverhulme Trust Research Leadership Award, in 2020 (one million GBP); the Young Scientist Award from the Electromagnetics Academy—Photonics and Electromagnetics Research Symposium, in 2021; and the Queen's University Belfast Vice Chancellor's Early Career Researcher Prize, in 2022. He serves as an Associate Editor for the IEEE Antennas and Wireless Propagation Letters. He has been a Guest Editor for several journals, including IEEE Antennas and Wireless Propagation Letters, IEEE Open Journal of Antennas and Propagation, and *Remote Sensing* (MDPI).